Materials Science-Poland, 33(3), 2015, pp. 508-514
http://www.materialsscience.pwr.wroc.pl/
DOI: 10.1515/msp-2015-0092

DE GRUYTER OPEN

Effects of Cr and Fe co-doping on structural, optical, electrical and magnetic properties of titanium dioxide (TiO_2)

SALMA WASEEM[1]*, SAFIA ANJUM[1], LUBNA MUSTAFA[1], ANUM DAR[2], FAROOQ BASHIR[2], REHANA ZIA[1]

[1]Department of Physics, Lahore College for Women University, Lahore, Pakistan
[2]Central Lab, Lahore College for Women University, Lahore, Pakistan

A series of $Ti_{0.9}Fe_{0.1-x}Cr_xO_2$ (where x = 0.0, 0.02, 0.04, 0.6, 0.08, 0.10) was synthesized using the powder metallurgy route. The structural, morphological, magnetic, optical and electrical properties were investigated by X-ray diffractometry (XRD), Raman spectroscopy, scanning electron microscopy (SEM), vibrating sample magnetometry (VSM), UV-Vis spectroscopy and four probe technique, respectively. The rutile phase was confirmed by XRD analysis which was also verified by Raman spectroscopy. It was observed that the grain size increased as the concentration of Cr increased. M-H loops extracted from VSM analysis revealed anti-ferromagnetic, weak ferromagnetic and paramagnetic behaviors at room temperature. The band gap energy and resistivity measurements exhibited the semiconducting nature of $Ti_{0.9}Fe_{0.1-x}Cr_xO_2$ based diluted magnetic semiconductors.

Keywords: *dilute magnetic semiconductors; rutile; grain size; magnetic properties; resistivity*

1. Introduction

Diluted magnetic semiconductors (DMS) consist of non magnetic semiconductor materials doped with a few atomic percent of transition metals. There are two types of DMS, i.e. II – VI and III – V compounds [1]. In recent years, II – VI compounds, i.e. oxide based diluted magnetic semiconductors (O-DMSs) have become the subject of a particular interest because both charge and spin degree of freedom play an important role in a single semiconductor material [2]. The magnetic interaction between magnetic ions via charge carriers provides a coupling between the charge and spin degree of freedom of electrons resulting in an improvement of structural, magnetic, optical and electrical properties [3].

O-DMSs with high Curie temperature have technological applications in the fields of optoelectronics, magnetoelectronics and microwave devices [4]. However, the origin of ferromagnetism in these oxide DMSs is still controversial as to whether it is caused by electron spins or it stems from magnetic precipitations due to dopant ions segregation [5].

Among oxide based diluted magnetic semiconductors (O-DMSs) titanium dioxide (TiO_2) presents interesting properties, such as transparency to visible light absorption, a wide band gap, high refractive index and low absorption. These properties are promising for applications such as catalysts, photoanodes, solar cells, magneto-optical devices [4]. TiO_2 is found in three crystalline forms: rutile, anatase and brookite. The band gaps of anatase and rutile phases of TiO_2 are 3.2 eV and 3 eV, respectively. Accordingly they show insulating behavior; however, by creating oxygen vacancy its conductivity can be increased [3].

Cr is an important dopant both from theoretical and experimental point of view as it has a major effect on carrier mobility. It appears to be a ferromagnetic dopant in thin films. It has been further reported that clusters of elemental Cr do

*E-mail: salma_ iqbal1990@hotmail.com

not give a ferromagnetic signal [6]. Among transition metal doped O-DMSs, Fe-doped TiO_2 materials have been analytically investigated. Most of the O-DMS research on Fe-doped TiO_2 was based on thin films or one-dimensional nanostructures, whereas a comprehensive analysis of the room temperature Fe-doped nanoparticles with various stoichiometries is missing [1].

A lot of work has been done on TiO_2 based DMS doped with a single transition metal but a little attention has been paid on co-dopants. Co-doping can lead to a remarkable improvement in properties of DMS. Chakrabari et al. reported that saturation magnetic field can be enhanced by adding 2 % of Fe in Co-ZnO system [7].

In the present work Fe and Cr have been used as co-dopants in TiO_2. The purpose of co-doping is to induce the room temperature ferromagnetism and to enhance charge carrier density in TiO_2. As a result, the magnetic and electrical properties of TiO_2 may be enhanced, which would improve its efficiency for DMS applications.

2. Experimental

2.1. Samples preparation

A series of six powder samples having general formula $Ti_{0.9}Fe_{0.1-x}Cr_xO_2$ (x= 0.00, 0.02, 0.04, 0.06, 0.08 and 0.10) has been prepared by powder metallurgy route. All the samples were weighed according to their stoichiometric ratio by using a precise electronic balance. After weighing all the samples were mixed and grinded individually by using a ceramic mortar and a pestle to get a homogenous mixture. These raw samples were then sintered in a heating furnace at 950 °C for 6 hours. Some of materials of prepared samples were used to make pellets for electrical resistivity measurement. A Carver pellet press was used to make disc shaped pellets of 1.3 mm diameter with acetone as a binder. The prepared pallets were then heated at 650 °C for 2 hours just for the purpose of hardening.

In this work crystal structure and phase identification of the samples were determined using X-ray diffractometer D-8 Discover, Bruker, made in Germany, having the source CuKα radiation with the wavelength $\lambda = 1.540598$ Å. UV-Vis analysis was done to study the variation of the band gap. The samples were examined optically by using UV 2800 model, Hitachi Japan, having wavelength of 300 to 900 nm. Surface morphology of the samples was observed through scanning electron microscope (SEM) using S-3400N Hitachi. Room temperature magnetic measurements were performed with a Lakeshore 7436 vibrating sample magnetometer. Electrical resistivity measurements were carried out by four probe technique at room temperature.

3. Results and discussion

3.1. XRD analysis

The comparative XRD patterns of the series $Ti_{0.9}Fe_{0.1-x}Cr_xO_2$ (x = 0, 0.02, 0.04, 0.06, 0.08 and 0.10) are shown in Fig. 1. All the peaks have been matched with JCPDS card number 21-1276 which has confirmed the rutile structure, i.e. tetragonal structure of the compound. There are some minor peaks of hematite phase for the value of x = 0.0, 0.02, 0.04, respectively. However these peaks vanish at x = 0.06, 0.08 and 0.1 respectively and a true rutile phase is developed. From these XRD micrographs, the most intense diffraction peak has been selected and lattice constants a and c were determined by the following relation [2]:

$$\frac{1}{d^2} = \frac{h^2 + k^2}{a^2} + \frac{l^2}{c^2} \qquad (1)$$

where d is the interplanar distance and hkl are the Miller indices of the corresponding plane. It is observed that as the concentration of Cr increases the values of lattice constants a and c decrease. The ionic radius of Cr^{2+} is 0.87 Å, of Fe^{2+} is 0.75 Å and of Ti^{+4} is 0.68 Å [8, 9]. The reason behind the decrease in the lattice constants is the incorporation of atoms with different sizes of ionic radii into TiO_2. These results are in agreement with the earlier findings [8]. The values of crystallite size (D), lattice constants a and c with varying concentration of x are given in Table 1.

Table 1. Values of crystallite size, lattice constants, grain size, band gap energy and resistivity of $Ti_{0.9}Fe_{0.1-x}Cr_xO_2$.

Cr x	Crystallite size D [nm]	Lattice constant a [nm]	Lattice constant c [nm]	Grain size [μm]	Eg [eV]	P [Ω·m]
0.0	61.45	0.458	0.296	2.1	2.2	1.48×10^{-8}
0.02	58.13	0.457	0.295	2.4	2.3	1.98×10^{-8}
0.04	57.90	0.457	0.294	2.5	2.3	2.21×10^{-8}
0.06	53.75	0.456	0.294	3.7	2.4	2.9×10^{-8}
0.08	53.06	0.454	0.293	3.9	2.5	3.01×10^{-8}
0.1	51.46	0.454	0.293	2.9	2.6	2.90×10^{-8}

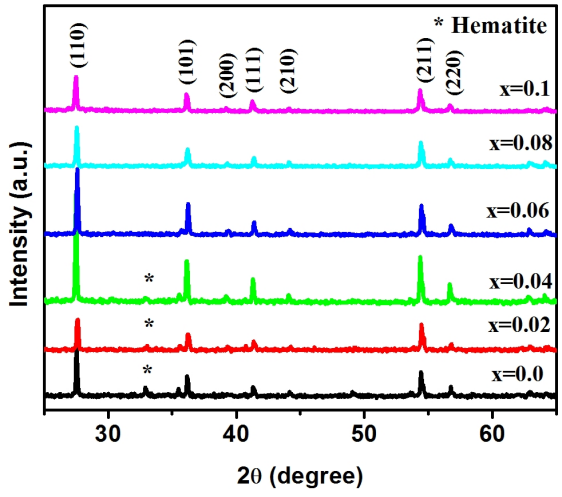

Fig. 1. Comparative XRD patterns of $Ti_{0.9}Fe_{0.1-x}Cr_xO_2$.

3.2. Raman spectroscopy analysis

Raman spectra of the series $Ti_{0.9}Fe_{0.1-x}Cr_xO_2$ are shown in Fig. 2. The thermodynamically stable rutile phase exhibits major peaks at 610, 446, and 242 cm^{-1} and minor peaks at 818, 707, and 319 cm^{-1} [10]. It is observed from the spectra that there are three most prominent peaks, i.e. at 264, 441 and 612 cm^{-1}, respectively. Usually, the four active Raman vibration modes of rutile phase are given by:

$$A_{1g} + B_{1g} + B_{2g} + Eg \qquad (2)$$

The peaks at 441 cm^{-1} and 612 cm^{-1} belong to E_g and A_{1g} mode respectively, whereas the peak at 264 cm^{-1} is known as a compound vibration peak due to multiple phonon scattering process. This peak is also known as the characteristic Raman peak of rutile TiO_2 [11]. The peaks corresponding to B_{1g}, at 143 cm^{-1} and B_{2g}, at 818 cm^{-1} are not observed due to technical limitations of the Raman device. There is a slight Raman shift in the observed values because of mixing of the dopants having different sizes of ionic radii with increased concentration of Cr.

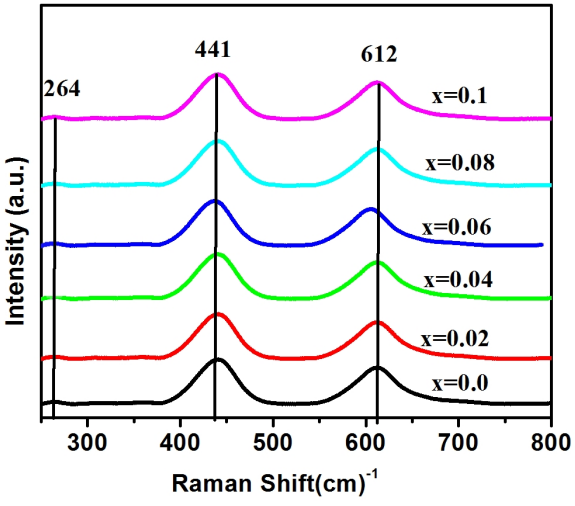

Fig. 2. Comparative Raman spectra of $Ti_{0.9}Fe_{0.1-x}Cr_xO_2$.

3.3. SEM analysis

The SEM micrographs of two samples at x = 0.04 and at x = 0.06 are shown in Fig. 3.

Well defined crystalline grains of uniform nature are observed in these micrographs. It is observed that the surface consists of large but homogenously distributed voids. From these graphs, an average grain size is measured by line intercept method. It is observed that the grain size increases with increased Cr concentration. The values of grain sizes are given in Table 1.

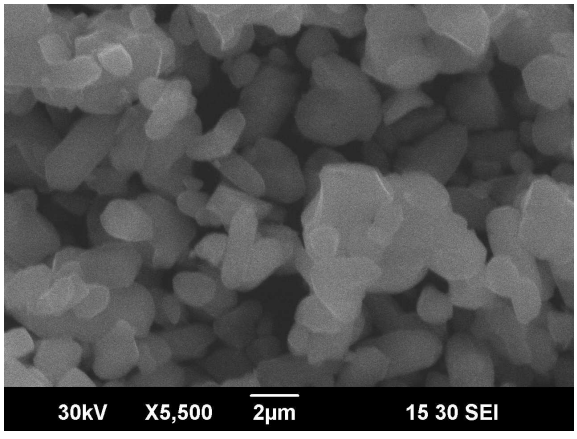

(a)

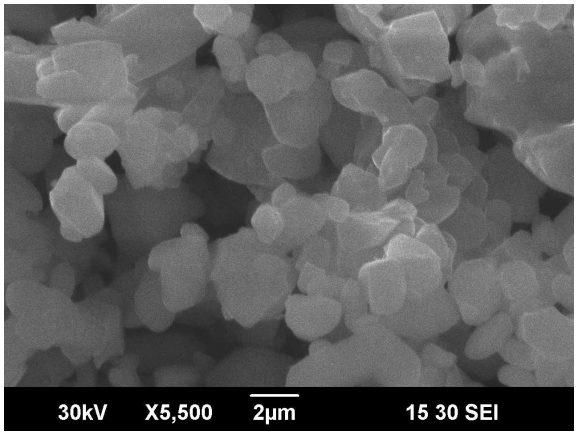

(b)

Fig. 3. SEM micrographs of $Ti_{0.9}Fe_{0.1-x}Cr_xO_2$ (a) x = 0.04 (b) x = 0.06.

3.4. VSM analysis

Hysteresis loops of $Ti_{0.9}Fe_{0.1-x}Cr_xO_2$ are shown in Fig. 4. The behavior of these loops drastically changes as the concentration of Cr increases. These loops show anti-ferromagnetic, weak ferromagnetic and paramagnetic behaviors at room temperature measurements. The M-H curves with the concentration of Cr at x = 0.0, 0.02, 0.04 are shown in Fig. 4a. It is revealed that these loops show antiferromagnetic behavior which may be due to the presence of hematite phase [12]. This phase is also confirmed by XRD micrographs.

As the concentration of Cr ions increases further up to 0.6, a weak ferromagnetic behavior is observed as shown in Fig. 4b. The value of magnetic moment increases due to the suitable ratio of Cr and Fe in TiO_2. Technically there are two main reasons for this increase in magnetization. First reason is the absence of the hematite phase since as it follows from the XRD micrograph, the pure rutile phase is achieved at this concentration. The second reason is the sp-d exchange interaction between the localized d shell of Cr and Fe atoms and delocalized sp orbital of the host (TiO_2) semiconductor [13].

With further increasing of Cr concentration, at x = 0.08 and 0.1, the paramagnetic behavior is observed as shown in Fig. 5c. The paramagnetic behavior may be due to large amount of Cr, i.e. 8 and 10 atomic percent and less amount of Fe, i.e. 2 and 0 atomic percent, respectively. As the concentration of Cr is large in these samples, so more spins are antiferomagnetically coupled. The sp-d exchange interaction decreases at this stage, resulting in paramagnetic behavior. It has been reported that addition of Cr to rutile TiO_2 above a certain amount, i.e. 6 atomic percent causes its paramagnetic behavior [6].

It is observed from M-H loops that coercivity of the series $Ti_{0.9}$ $Fe_{0.1-x}Cr_xO_2$ decreases from x = 0.00 to 0.1. Coercivity depends upon grain size. As the concentration of Cr increases, the grain size increases as is observed from the SEM analysis, so the number of domain walls decreases and less reversal magnetizing force may demagnetize the material [14].

3.5. UV-Vis analysis

The plots of $(\alpha h\nu)^2$ versus band gap energy (E_g) of the series of $Ti_{0.9}Fe_{0.1-x}Cr_xO_2$ are shown in Fig. 5. The band gap energy E_g is determined by Tauc's equation [15] given as:

$$\alpha(h\nu) = A(h\nu - E_g)^m \tag{3}$$

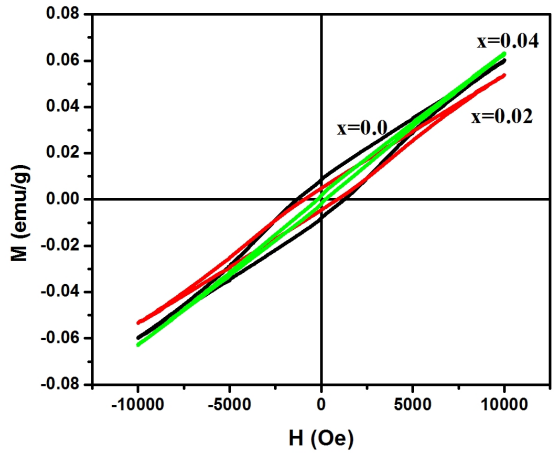

(a)

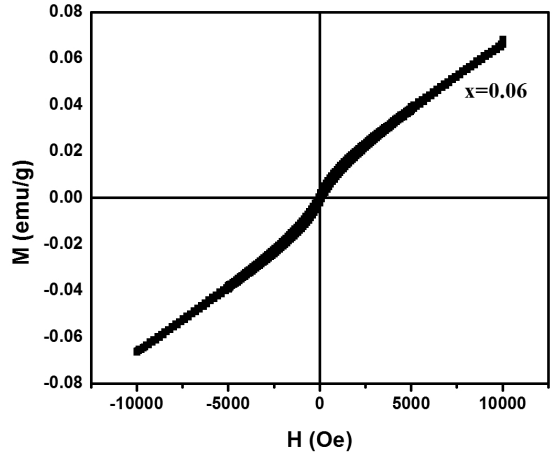

(b)

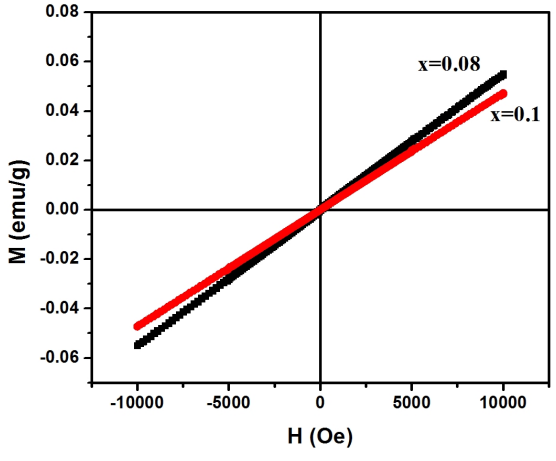

(c)

Fig. 4. Hysteresis loops of $Ti_{0.9}Fe_{0.1-x}Cr_xO_2$ (a) x = 0.0, 0.02, 0.04 (b) x = 0.06 (c) x = 0.08, 0.1.

where α is the absorption coefficient, $h\nu$ is the photon energy, E_g is band gap energy and A is a constant known as a band tailing parameter which is different for different material. The magnitude of m is characteristic of the type of transition and takes the value 1/2, 3/2, 2 and 3 for direct, allowed forbidden, indirect allowed and indirect forbidden transitions, respectively. The linear part of the curves is extrapolated to $\alpha = 0$ to get direct band gap energy. It is observed that band gap energy (E_g) increases as the concentration of Cr increases. It is due to the fact that as the impurities are added to a semiconductor some impurity levels are developed within the band gap which increases the band gap [1]. These results are in agreement with the earlier experimental studies [16].

3.6. Electrical resistivity measurements

The plot of resistivity versus concentration of Cr of the series $Ti_{0.9}$ $Fe_{0.1-x}Cr_xO_2$ is shown in Fig. 6. From the resistivity measurements it is observed that as the concentration of Cr increases, resistivity increases but the range of resistivity is typical of semiconductors. The increase in resistivity can be attributed to an increase in band gap as is observed from UV-Vis analysis. The variation of resistivity versus Cr concentration is shown in Table 1.

4. Conclusions

The $Ti_{0.9}Fe_{0.1-x}Cr_xO_2$ based DMS have been fabricated by powder metallurgy route. Structural properties confirmed the formation of rutile phase of TiO_2. Different kinds of magnetic behaviors, including anti-ferromagnetic, weak ferromagnetic and paramagnetic were observed by VSM analysis at room temperature. The prepared DMS lie in the semiconducting range which has been confirmed by resistivity measurements and UV-Vis analysis. At x = 0.06, no secondary phase of hematite was found and at room temperature ferromagnetic behavior was also observed. From this we can conclude that the co-doping improved the structural, magnetic and electrical properties of co-doped $Ti_{0.9}Fe_{0.1-x}Cr_xO_2$. So, $Ti_{0.9}Fe_{0.04}Cr_{0.06}O_2$

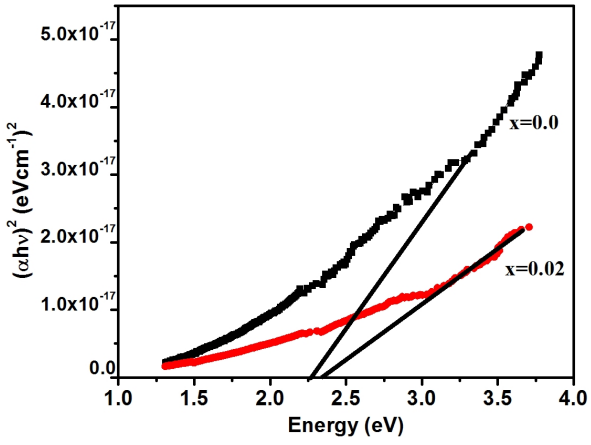

(a)

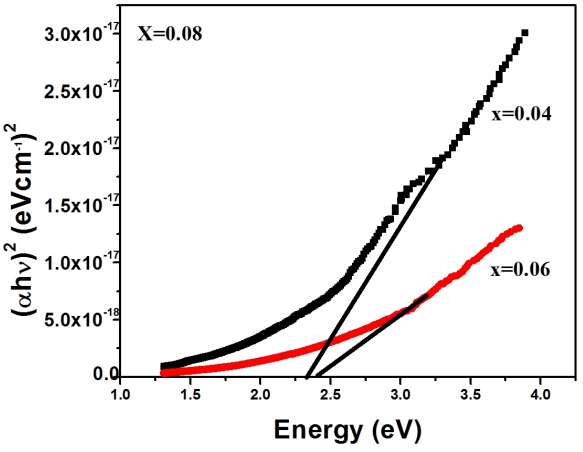

(b)

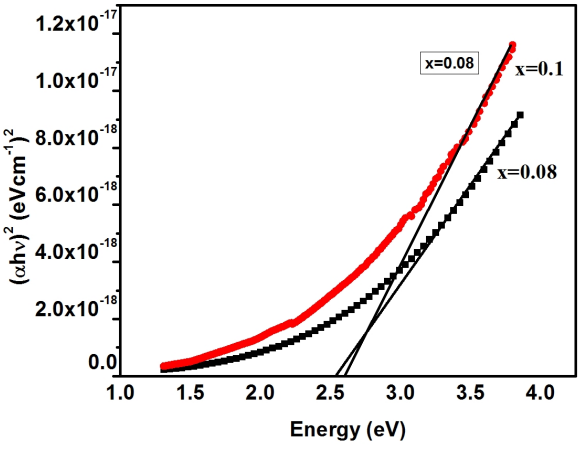

(c)

Fig. 5. Band gap energy of $Ti_{0.9}Fe_{0.1-x}Cr_xO_2$ (a) x = 0.0, x = 0.02 (b) x = 0.04, 0.06 (c) x = 0.08, 0.1.

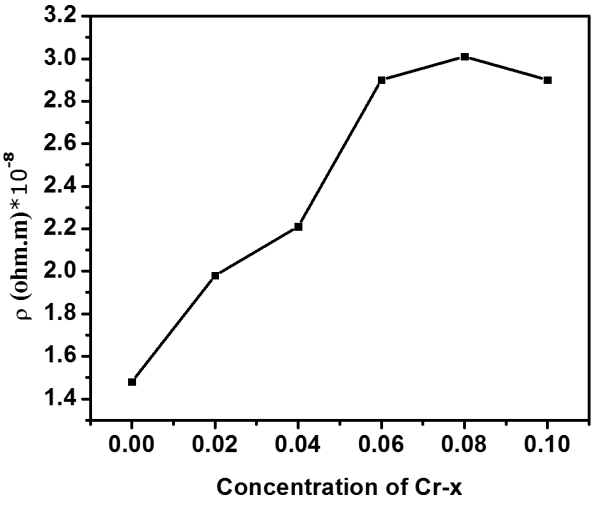

Fig. 6. Dependence of electrical resistivity on Cr concentration for $Ti_{0.9}Fe_{0.1-x}Cr_xO_2$.

was optimized value for practical spintronics applications.

Acknowledgements

The authors would like to thank Dr Hafza Khusrhid, University of South Florida Tampa Florida, USA, for her technical support.

References

[1] KIRIT S., DIMPLE S., *J. Cryst. Growth*, 352 (2012), 224.

[2] PATEL S., KURIAN S., GAJBHIYE N., *J. Mater. Res. Bull.*, 48 (2013), 655.

[3] BAPNA K., CHOUDHARY R., PHASE D., *J. Mater. Res. Bull.*, 47 (2012), 2001.

[4] BOUAINE A., SCHMERBER G., IHIAWAKRIM D., DERORY A., *Mater. Sci. Eng. B-Adv.*, 177 (2012), 1618.

[5] LU X., LI J., MOU X., WU J., DING S, HUANG F., *J. Alloy. Compd.*, 499 (2010), 160.

[6] KOOHPAYEH S., WILLIAMS A., ABELL J., LIM J., BLACKBURN E., *J. Appl. Phys.*, 108 (2010), 073919.

[7] CHAKRABARTI M., DECHOUDHURY D., SENYAL T., ROY K., BHOWMICK D., CHAKRABARTI A., *J. Phys. D*, 41 (2008), 135006.

[8] PING XU., LAN LI., LI-YA LV., XIAO-SONG Z., XI-MING C., JIAN-FENG W., FENG-MING Z., WEI Z., SYOU-WEI D., *Chin. Phys. Lett.*, 26 (2009), 097502.

[9] SHANNON R.D., *Acta Cryst.* A, 32 (1976), 751.

[10] HARDCASTLE F.D., *J. Ark. Acad. Sci.*, 65 (2011), 43.

[11] TOSHIAKI O., FUJIO I., YOSHINORI F., *J. Raman Spectrosc.*, 7 (1978), 321.

[12] TANG H., PRASAD K., SANJINES R., SCHMID P.E., LEVY F., *J. Appl. Phys.*, 75 (1994), 2042.

[13] SALEEM M., SIDDIQUI A.S. ATIQ S., ANWAR S., RIAZ S., *Chin. J. Chem. Phys.*, 23 (2010), 469.

[14] ANJUM S., RASHID A., BASHIR F., RIAZ S., PERVAIZ M., ZIA R., *IEEE Trans. Magn.*, 50 (2014), 2200504.

[15] TAUC J., GRIGOROVICI R., VANCU A., *Phys. Status Solidi*, 15 (1966), 627.

[16] JEONG E.D., BORSE P.H., JANG J.S., LEE J.S., JUNG K., CHANG H., JIN J.S., WON M.S., KIM H.G., *J. Ceram. Process. Res.*, 9 (2008), 250.

Received 24-09-2014
Accepted 17-06-2015